



Layer-dependent electronic structure of an atomically heavy two-dimensional dichalcogenide

Po-Chun Yeh,¹ Wencan Jin,² Nader Zaki,² Datong Zhang,² Jonathan T. Liou,¹ Jerzy T. Sadowski,³ Abdullah Al-Mahboob,³ Jerry I. Dadap,² Irving P. Herman,² Peter Sutter,³ and Richard M. Osgood, Jr.^{1,2,*}

¹*Department of Electrical Engineering, Columbia University, New York, New York 10027, USA*

²*Department of Applied Physics and Applied Mathematics, Columbia University, New York, New York 10027, USA*

³*Center for Functional Nanomaterials, Brookhaven National Laboratory, Upton, New York 11973, USA*

(Received 9 July 2014; published 20 January 2015)

We report angle-resolved photoemission spectroscopic measurements of the evolution of the thickness-dependent electronic band structure of the atomically heavy two-dimensional layered dichalcogenide, tungsten diselenide (WSe₂). Our data, taken on mechanically exfoliated WSe₂ single crystals, provide direct evidence for shifting of the valence-band maximum from $\bar{\Gamma}$ (multilayer WSe₂) to \bar{K} (single-layer WSe₂). Further, our measurements also set a lower bound on the energy of the direct band gap and provide direct measurement of the hole effective mass.

DOI: [10.1103/PhysRevB.91.041407](https://doi.org/10.1103/PhysRevB.91.041407)

PACS number(s): 79.60.Bm, 61.05.jh, 68.37.Nq, 71.18.+y

Single layers of two-dimensional metal dichalcogenides (TMDCs) such as MoS₂ have emerged as a new class of noncentrosymmetric direct-band-gap materials with potential photonic and spintronic applications [1,2]. Among the TMDC family, tungsten-based dichalcogenides, such as WSe₂, exhibit high in-plane carrier mobility and allow electrostatic modulation of the conductance [3,4], characteristics that make them promising for device applications. For example, bulk WSe₂ possesses an indirect band gap of 1.2 eV [1,5] and has been used as the channel of a field-effect transistor (FET) with an intrinsic hole mobility of up to 500 cm²/(V s) [6]. By comparison, WSe₂, in its monolayer form (ML), should have a direct band gap, as predicted by theory [7–12], and a promising intrinsic hole mobility of 250 cm²/(V s), as recently demonstrated in the performance of top-gated FETs [4]. In addition, ML WSe₂ has been demonstrated to be the first TMDC material possessing ambipolar, i.e., both *p*-type and *n*-type, conducting behavior [4,12], thus making it possible to design additional electronic functionality, such as *p*–*n* junctions or complementary logic circuits.

Despite these intriguing characteristics, measurements of ML WSe₂ have generally been limited to probing of optical and transport properties [4–6]. In this Rapid Communication, we report thickness-dependent measurements of the surface and electronic structure of exfoliated WSe₂, using low-energy electron microscopy (LEEM), diffraction (LEED), and micrometer-scale angle-resolved photoemission spectroscopy (μ -ARPES) of samples supported on a native-oxide-terminated silicon substrate. Our experimental results provide direct evidence for a predicted valence-band maximum (VBM) symmetry-point change, which leads to an indirect-to-direct band-gap transition. Because TMDCs have a large carrier effective mass and reduced screening in two dimensions, electron-hole interactions are much stronger than in conventional semiconductors [13–15]. Our results allow us to obtain a direct measurement of the hole effective mass. Finally, our measurements allow us to directly infer a lower bound on the energy of the direct band gap.

Our measurements were performed using the spectroscopic photoemission and low-energy electron microscope (SPE-LEEM) system at the National Synchrotron Light Source (NSLS) beamline U5UA [16,17]. The spectrometer energy

resolution of this instrument was set to 100 meV at 33 eV incident photon energy with a beam spot size of 1 μ m in diameter. The momentum resolution is $\sim 0.02 \text{ \AA}^{-1}$. Exfoliated WSe₂ samples were transferred to a native-oxide covered Si substrate; prior to measurements, these samples were annealed at 350 °C for ~ 12 h under UHV conditions. The layer number of the sample is determined by Raman and photoluminescence spectroscopy [18,19]. Additional experimental details can be found in the Supplemental Material [20], which includes Refs. [21,22].

Sample quality and crystal orientation were examined using both LEEM and μ -LEED (Fig. 1). Diffraction patterns (at a primary electron energy of 48 eV) of exfoliated WSe₂ flakes of 1–3ML and bulk are shown in Figs. 2(a)–2(d), respectively, and clearly display the sixfold crystal symmetry. At an electron energy of 48 eV, the mean free path of the low-energy electrons is $\sim 5.2 \text{ \AA}$ [23], which is comparable to the thickness of a single covalently bound Se-W-Se unit of monolayer WSe₂ ($\sim 7 \text{ \AA}$) [4,24]. With increasing WSe₂ thickness, the LEED spots become sharper, due in part to decreased scattering from the substrate [25]. This assertion is supported by the monotonically decreasing full width at half maximum (FWHM) of the (00) diffraction spot, plotted for different electron energies in Fig. 2(e) [25].

The electronic structure of the top-lying valence bands of WSe₂ is derived from the W 5*d* and Se 4*p* orbitals [26,27], each of which possesses a strongly varying photon-energy-dependent photoionization cross section [28], as displayed in Fig. 3(b). Prior work [28] has shown that the cross section of the W 5*d* subshell is an order of magnitude larger than that of Se 4*p* at the photon energy of 33 eV used in our experiments [indicated by the vertical line in Fig. 3(b)]. Thus the primary contributions to our μ -ARPES measurements, shown in Fig. 4, are from the W 5*d* orbitals. Angle-integrated photoemission spectra of 1 ML WSe₂ along high-symmetry directions and over the full Brillouin zone (BZ) are shown in Fig. 3(c). These spectra show a clear energy cutoff at about 1.8 ± 0.1 eV above the VBM, which we identify as the position of the Fermi level E_F . The band gap of ML WSe₂ has been previously reported to be in the range of 1.4–2.3 eV [19,29,30]. Based on our identification of the Fermi energy, the minimum band-gap value of WSe₂ must be greater than at least 1.8 eV; this

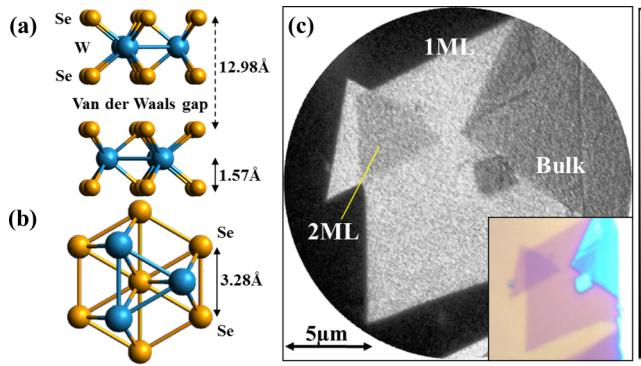


FIG. 1. (Color online) (a) Side view and (b) top view of the trigonal prismatic coordination of the atoms in 2H-WSe₂. (c) LEEM image of 1 ML WSe₂ after transfer (detector artifacts and background signal have been removed.) The inset is the corresponding optical microscope image of the same sample. LEEM images were taken at an electron energy of 1.8 eV.

result also suggests that our exfoliated ML WSe₂ is heavily electron doped, i.e., the Fermi level falls near the conduction-band minimum [31,32]. The energy differences between the Fermi level (E_F) and the VBM for 2 ML, 3 ML, and bulk are approximately 1.5, 1.5, and 1.1 eV, respectively. Taking into account the previously reported band-gap energies of these materials, we find that these energy differences are consistent with our samples being heavily electron doped, regardless of thickness. This result suggests that our electron doping is more likely to be intrinsic to the layered material and not due to charge transfer from the substrate.

Our μ -ARPES measurements of 1–3 ML and bulk WSe₂ along the high-symmetry directions $\bar{M} - \bar{\Gamma} - \bar{K}$, given in Fig. 4, clearly show a transition in the occupied electronic structure with a change in layer thickness. Superimposed on the measured data are the corresponding density functional theory–local density approximation (DFT-LDA) band calculations, computed using ABINIT without a spin-orbit interaction [33,34]. In the spectra, the distinctive features include the VBM at $\bar{\Gamma}$, derived from the W d_{z^2} and Se p_z orbitals, the VBM at \bar{K} , derived from the W $d_{x^2-y^2}/d_{xy}$ and Se p_x/p_y orbitals, and the valley between $\bar{\Gamma}$ and \bar{K} , derived from a crossover to the W $d_{x^2-y^2}/d_{xy}$ orbitals from the W d_{z^2} and Se p_z orbitals [11,35,36], as shown and labeled in Fig. 4(a). Bands of higher binding energies and along other high-symmetry directions have been previously calculated and discussed in the literature

[11,26,27,35–37]. These features are further displayed in the corresponding energy distribution curves (EDCs) [see Fig. 4(b)] and momentum distribution curves (MDCs) [see Fig. 4(c)]. Note that several of the WSe₂ bands are not detected in our ARPES measurements due to matrix-element selection rules as well as the above-mentioned difference in the photoionization cross section between W- and Se-derived states. In our experiments, the incident photon flux was directed normal to the sample surface so that its polarization is in the plane of the WSe₂ crystal, thus suppressing excitation of states with out-of-plane character. This result explains why the W- and Se-derived states with a z or out-of-plane component, i.e., d_{z^2} or p_z orbital, in the uppermost valence band (UVB) near $\bar{\Gamma}$ have a consistently relatively weaker, but nonzero, intensity for 1–3 ML and bulk WSe₂.

An important feature of our measurements is the change in the energy of the uppermost valence band (UVB) at $\bar{\Gamma}$ and \bar{K} for 1 ML WSe₂ compared to that of few-layer WSe₂. Our μ -ARPES spectra show that the valence-band maximum is at \bar{K} for 1 ML WSe₂ and shifts to $\bar{\Gamma}$ for multilayer WSe₂. Previous reports [38–42] using traditional ARPES and inverse photoemission instruments have confirmed that the location of the VBM in bulk WSe₂ is at $\bar{\Gamma}$; note that for bulk WSe₂, ARPES measurements over a large enough photon energy range are required in order to take into account the k_z dependence of the observed states. To fully quantify the VBM transition as a function of thickness, we used curvature analysis [43], or the second-derivative method, to help delineate the electronic band structure, as shown in Fig. 5. Figures 5(a)–5(d) give the bands for the 1–3 ML and bulk WSe₂ samples, derived from the data in Fig. 4 using this method, and with the zero energy referenced to the VBM. The UVB of exfoliated WSe₂ closely matches the corresponding calculated bands (white curves), except for the monolayer case, where the measured energy difference between $\bar{\Gamma}$ and \bar{K} is less than that predicted by theory, and where the dispersion at $\bar{\Gamma}$ is greater than that in the calculated bands. The experimentally measured and theoretically predicted [11] energy differences between $\bar{\Gamma}$ and \bar{K} for monolayer and multilayer WSe₂ are plotted in Fig. 5(e). The measured energy differences are 0.21, -0.14 , and -0.25 eV for 1–3 ML; the value for bulk WSe₂ has been reported previously to be -0.3 eV [39,41]. The error bars denote the standard deviation of the fittings from all six high-symmetry equivalent directions, and they are well under the detector error of ± 0.10 eV. Thus, these results provide direct experimental evidence for a thickness-dependent shift

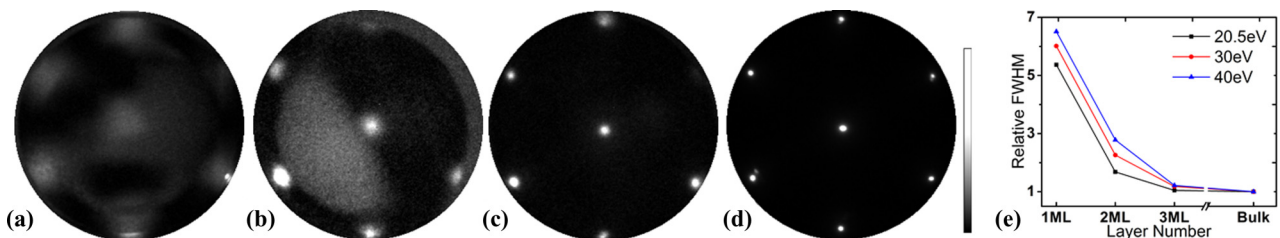


FIG. 2. (Color online) (a)–(d) LEED patterns at 48 eV electron energy on exfoliated WSe₂ (a) 1 ML, (b) 2 ML, (c) 3 ML, and (d) bulk after transfer to Si. The halo around the 1 ML (00) spot came from the edge deflection of electrons due to a limited sample size. (e) Measured FWHM of the (00) LEED spot for 1–3 ML WSe₂ flakes relative to that of bulk, measured at 20.5, 30, and 40 eV electron energy. The FWHM decreases with an increasing number of layers, since electrons elastically backscattered from the Si substrate are progressively decreased.

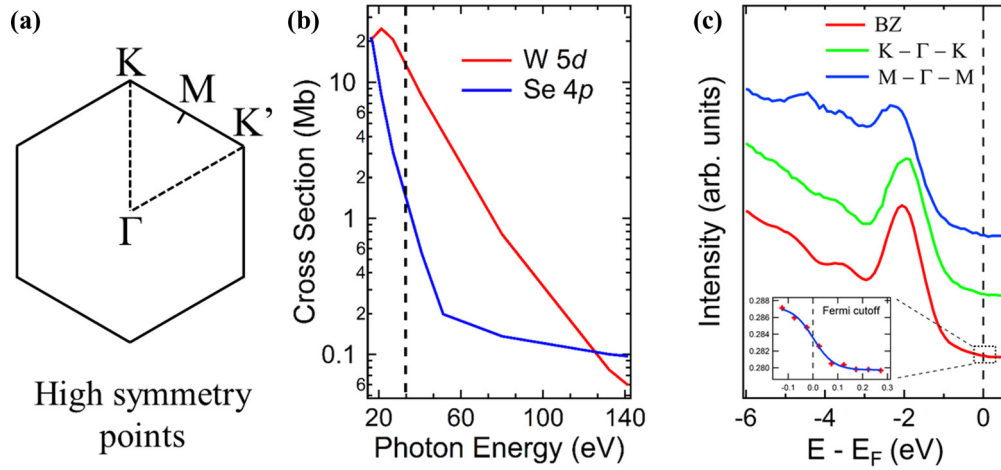


FIG. 3. (Color online) (a) Brillouin zone and high-symmetry points of WSe_2 . (b) Atomic photoionization cross section for W 5d and Se 4p subshells as a function of ARPES photon energy [28]. At 33 eV, the cross section between W 5d and Se 4p has an order-of-magnitude difference. Therefore, the dominant features in our ARPES measurement are the contribution of the W 5d subshell. Note that the Cooper minimum of the Se orbital is ~ 50 eV. (c) Angle-integrated photoemission spectra of monolayer WSe_2 extracted from high-symmetry directions $K-\Gamma-K$ and $M-\Gamma-M$, and over the full BZ, referenced with respect to the Fermi level.

in the relative energy of the VBM at $\bar{\Gamma}$ and at \bar{K} and, hence, strong support for a shift from an indirect to a direct band gap in going from 2 to 1 ML WSe_2 .

An analysis of the curvature of the bands from the μ -ARPES measurements also allows us to deduce the effective mass of monolayer and bilayer WSe_2 . For monolayer WSe_2 , we determined an experimentally derived hole effective mass of

$1.4 \pm 0.6m_0$ [44] (where m_0 is the electron mass) at \bar{K} , which is $\sim 3\times$ larger than theoretical predictions, and a hole effective mass of $3.5 \pm 1.8m_0$ [44] at $\bar{\Gamma}$. The latter quantity is approximately half as large as theoretical predictions ($7.1 \pm 0.2m_0$) [7–10,45]. For the case of bilayer WSe_2 , however, we determined an experimentally derived hole effective mass of $0.4 \pm 0.1m_0$ at \bar{K} , which agrees well with theoretical predictions

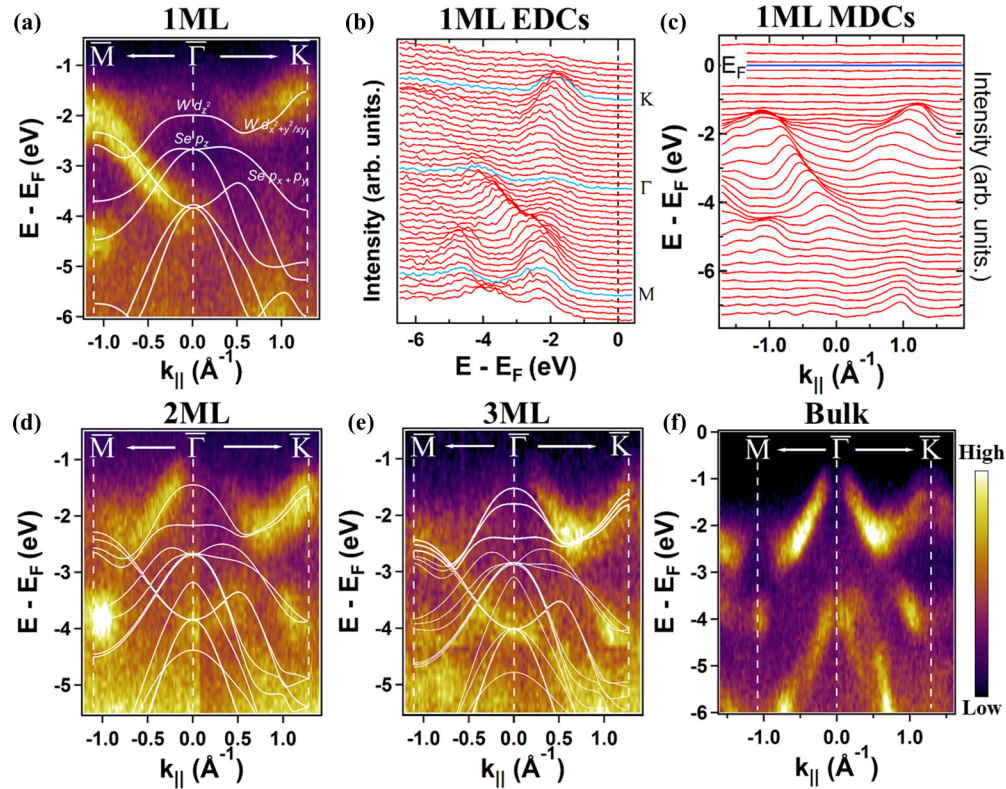


FIG. 4. (Color online) μ -ARPES band mapping of exfoliated WSe_2 for (a) 1 ML, (d) 2 ML, (c) 3 ML, and (f) bulk along the high-symmetry path $M-\Gamma-K$ in the Brillouin zone. $E = 0$ denotes the Fermi level. The overlaid white lines are our DFT-calculated band structures. The calculations do not include the effect of spin-orbit coupling. (b), (c) Corresponding EDCs and MDCs of 1 ML WSe_2 , respectively.

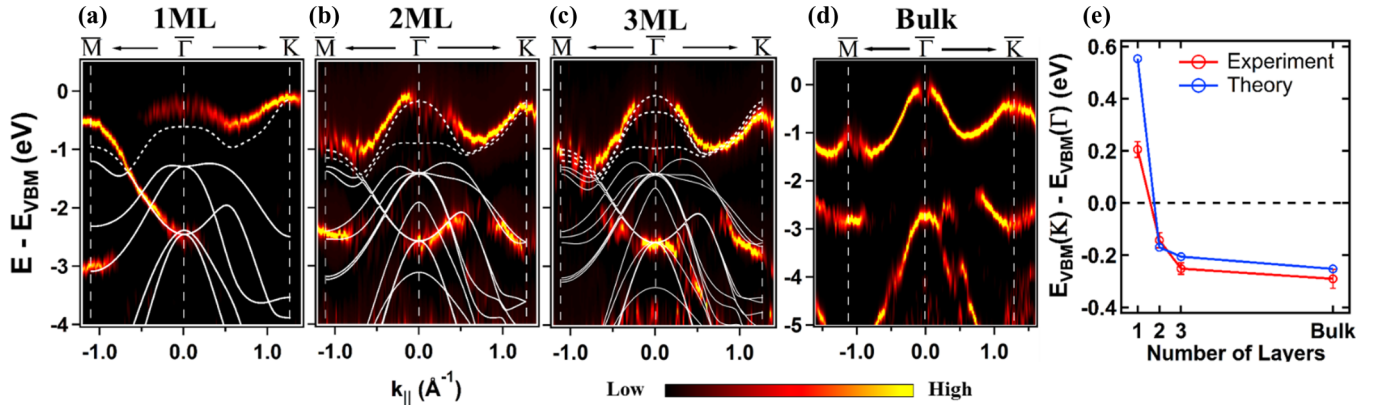


FIG. 5. (Color online) (a)–(d) Second derivatives of the low-energy valence bands along high-symmetry points of exfoliated 1–3 ML and bulk WSe_2 , respectively, generated from the μ -ARPES band maps of Fig. 4. The white lines are the corresponding DFT-calculated bands as in Fig. 4. The dashed white lines refer to the top valence bands, which illustrate the layer-number dependence of the electronic structure near the VBM. Here the energy scale is set to zero at the VBM. (e) Layer-number-dependent VBM transition in terms of the energy difference between K and Γ points. The error bars denote the standard deviation of the fittings from all six high-symmetry equivalent directions, and they are well under the detector error of ± 0.10 eV. The theoretical and experimental results are plotted for comparison.

[7,9]. The origin of the discrepancy between experiment and DFT calculations for the case of a monolayer is uncertain at this time. Our finite energy resolution does contribute to the measurement error. However, it is also apparent that there is an overall difference in band dispersion between our relatively simple theory calculation and experiment. This reasoning indicates that the above discrepancy is more complicated than simple instrumentation limits. Note that our DFT-derived effective mass value of $0.44m_0$ for monolayer WSe_2 at \bar{K} is in reasonable agreement with previous theoretical reports [7–10]. Also, since $m_{\text{eff}} \propto |\frac{\partial^2 E}{\partial k^2}|^{-1}$, slight measurement errors are accentuated by the flatlike dispersion curve in the vicinity of $\bar{\Gamma}$. “Renormalization” in bands of other two-dimensional (2D) dichalcogenides have also been reported [46,47], though the reason for this remains in question. Other possible explanations beyond that of an intrinsic nature of WSe_2 include effects of substrate interaction, such as strain, dielectric screening, etc.

In comparison to monolayer MoS_2 , monolayer WSe_2 is expected to have an even larger spin-orbit splitting in the vicinity of \bar{K} , with a theoretically predicted value of ~ 0.46 eV vs ~ 0.16 eV of MoS_2 [11,48]. The expected splitting of the valence band along the $\bar{\Gamma} - \bar{K}$ direction of monolayer WSe_2 is due to the strong spin-orbit coupling originating from the high mass of the constituent elements and the lack of inversion symmetry [11,48–50]. The theoretically predicted value (~ 0.46 eV) is larger than our experiment energy resolution and thus should have been resolved directly in our measurements. However, despite the presence of an increasing linewidth of the UVB in the direction of $\bar{\Gamma} - \bar{K}$, which may be attributed to spin-orbit splitting of the bands, we do not see two clear peaks in the vicinity of \bar{K} . We conjecture that the sample roughness, induced in the transfer process, is broadening the linewidth [51] of the spin-orbit split bands, leading to a broad unresolved band in our ARPES measurements. We have shown in previous works [25,47], using an analysis of LEED spot widths, that the transfer process introduces corrugation in monolayer MoS_2 . Thus, resolving the spin-orbit splitting in monolayer dichalcogenides is demanding in terms of a flat transfer procedure.

In conclusion, we have probed the surface structure and occupied electronic bands of one- to three-layer exfoliated WSe_2 crystals prepared by transfer to a native-oxide-terminated Si substrate. LEEM and μ -LEED provided real-space and reciprocal-space structural measurements of WSe_2 , revealing clearly resolved thickness-dependent contrast and diffraction spot widths, respectively. Our μ -ARPES measurements have probed the occupied valence-band structure and confirmed the transition of the valence-band maximum from $\bar{\Gamma}$ to \bar{K} as the thickness is reduced from few-layer to 1 ML WSe_2 ; this observation provides support for an indirect-to-direct band-gap transition. For monolayer WSe_2 , we have found a lower bound of 1.8 eV for the band gap and measured a hole effective mass of $1.4m_0$ at \bar{K} and $3.5m_0$ at $\bar{\Gamma}$. We expect that these results will provide insight for understanding the optical and electronic properties of monolayer and multilayer WSe_2 that is important for devices made from this transition-metal dichalcogenide material.

The beamline measurements and analyses and the sample mounting were supported by the Department of Energy, Office of Basic Energy Sciences, Division of Materials Sciences and Engineering under Award Contract No. DE-FG 02-04-ER-46157 and were carried out in part at the Center for Functional Nanomaterials and National Synchrotron Light Source, Brookhaven National Laboratory, which is supported by the U.S. Department of Energy, Office of Basic Energy Sciences, under Contract No. DE-AC02-98CH10886. The sample preparation and optical characterization (by D.Z., J.T.L., and I.P.H.) was supported as part of the Center for Re-Defining Photovoltaic Efficiency through Molecular Scale Control, an Energy Frontier Research Center funded by the U.S. Department of Energy (DOE), Office of Science, Office of Basic Energy Sciences under Award No. DE-SC0001085. The EFRC work is also supported by a matching grant from the Empire State Development’s Division of Science, Technology and Innovation (NYSTAR) as well as by the New York State Energy Research Development Authority (NYSERDA).

- [1] K. F. Mak, C. Lee, J. Hone, J. Shan, and T. F. Heinz, Atomically thin MoS₂: A new direct-gap semiconductor, *Phys. Rev. Lett.* **105**, 136805 (2010).
- [2] A. Splendiani, L. Sun, Y. Zhang, T. Li, J. Kim, C.-Y. Chim, G. Galli, and F. Wang, Emerging photoluminescence in monolayer MoS₂, *Nano Lett.* **10**, 1271 (2010).
- [3] D. Braga, I. Gutiérrez Lezama, H. Berger, and A. F. Morpurgo, Quantitative determination of the band gap of WS₂ with ambipolar ionic liquid-gated transistors, *Nano Lett.* **12**, 5218 (2012).
- [4] H. Fang, S. Chuang, T. C. Chang, K. Takei, T. Takahashi, and A. Javey, High-performance single layered WSe₂*p*-FETs with chemically doped contacts, *Nano Lett.* **12**, 3788 (2012).
- [5] G. H. Yousefi, Optical properties of mixed transition metal dichalcogenide crystals, *Mater. Lett.* **9**, 38 (1989).
- [6] V. Podzorov, M. E. Gershenson, Ch. Kloc, R. Zeis, and E. Bucher, High-mobility field-effect transistors based on transition metal dichalcogenides, *Appl. Phys. Lett.* **84**, 3301 (2004).
- [7] A. Kumar and P. K. Ahluwalia, Electronic structure of transition metal dichalcogenides monolayers 1H-*MX*₂ (*M* = Mo, W; *X* = S, Se, Te) from *ab-initio* theory: New direct band gap semiconductors, *Eur. Phys. J. B* **85**, 186 (2012)
- [8] A. Ramasubramaniam, Large excitonic effects in monolayers of molybdenum and tungsten dichalcogenides, *Phys. Rev. B* **86**, 115409 (2012).
- [9] W. S. Yun, S. W. Han, S. C. Hong, I. G. Kim, and J. D. Lee, Thickness and strain effects on electronic structures of transition metal dichalcogenides: 2H-*MX*₂ semiconductors (*M* = Mo, W; *X* = S, Se, Te), *Phys. Rev. B* **85**, 033305 (2012).
- [10] H. Shi, H. Pan, Y.-W. Zhang, and B. I. Yakobson, Quasiparticle band structures and optical properties of strained monolayer MoS₂ and WS₂, *Phys. Rev. B* **87**, 155304 (2013).
- [11] Z. Y. Zhu, Y. C. Cheng, and U. Schwingenschlög, Giant spin-orbit-induced spin splitting in two-dimensional transition-metal dichalcogenide semiconductors, *Phys. Rev. B* **84**, 153402 (2011).
- [12] W. Liu, J. Kang, D. Sarkar, Y. Khatami, D. Jena, and K. Banerjee, Role of metal contacts in designing high-performance monolayer *n*-type WSe₂ field effect transistors, *Nano Lett.* **13**, 1983 (2013).
- [13] A. M. Jones, H. Yu, N. J. Ghimire, S. Wu, G. Aivazian, J. S. Ross, and B. Zhao, Optical generation of excitonic valley coherence in monolayer WSe₂, *Nat. Nanotechnol.* **8**, 634 (2013).
- [14] K. F. Mak, K. He, C. Lee, G. H. Lee, J. Hone, T. F. Heinz, and J. Shan, Tightly bound trions in monolayer MoS₂, *Nat. Mater.* **12**, 207 (2013).
- [15] J. S. Ross, S. Wu, H. Yu, N. J. Ghimire, A. M. Jones, G. Aivazian, J. Yan *et al.*, Electrical control of neutral and charged excitons in a monolayer semiconductor, *Nat. Commun.* **4**, 1474 (2013).
- [16] J. T. Sadowski, Pentacene growth on 3-aminopropyl-trimethoxysilane modified silicon dioxide, *Opt. Mater.* **34**, 1635 (2012).
- [17] P. Sutter, M. S. Hybertsen, J. T. Sadowski, and E. Sutter, Electronic structure of few-layer epitaxial graphene on Ru(0001), *Nano Lett.* **9**, 2654 (2009).
- [18] H. Zeng, G.-B. Liu, J. Dai, Y. Yan, B. Zhu, R. He, and L. Xie, Optical signature of symmetry variations and spin-valley coupling in atomically thin tungsten dichalcogenides, *Sci. Rep.* **3**, 1608 (2013).
- [19] W. Zhao, Z. Ghorannevis, L. Chu, M. Toh, C. Kloc, P.-H. Tan, and G. Eda, Evolution of electronic structure in atomically thin sheets of WS₂ and WSe₂, *ACS Nano* **7**, 791 (2013).
- [20] See Supplemental Material at <http://link.aps.org/supplemental/10.1103/PhysRevB.91.041407> for more details about sample preparation, ARPES configuration, and matrix-element analysis.
- [21] J. I. Flege, E. Vescovo, G. Nintzel, L. H. Lewis, S. Hulbert, and P. Sutter, A new soft x-ray photoemission microscopy beamline at the National Synchrotron Light Source, *Nucl. Instrum. Methods B* **261**, 855 (2007).
- [22] P. Sutter and E. Sutter, Microscopy of graphene growth, processing, and properties, *Adv. Funct. Mater.* **23**, 2617 (2013).
- [23] M. P. Seah and W. A. Dench, Quantitative electron spectroscopy of surfaces: A standard data base for electron inelastic mean free paths in solids, *Surf. Interface Anal.* **1**, 2 (1979).
- [24] V. L. Kalikhman and Y. S. Umanskii, Transition-metal chalcogenides with layer structure and features of the filling of their Brillouin zones, *Sov. Phys. Usp.* **15**, 728 (1973).
- [25] P.-C. Yeh, W. Jin, N. Zaki, D. Zhang, J. T. Sadowski, A. Al-Mahboob, A. M. van der Zande, D. A. Chenet, J. I. Dadap, I. P. Herman, P. Sutter, J. Hone, and R. M. Osgood, Jr., Probing substrate-dependent long-range surface structure of single-layer and multilayer MoS₂ by low-energy electron microscopy and microprobe diffraction, *Phys. Rev. B* **89**, 155408 (2014).
- [26] L. Mattheiss, Band structures of transition-metal-dichalcogenide layer compounds, *Phys. Rev. B* **64**, 235305 (2001).
- [27] R. Coehoorn, C. Haas, J. Dijkstra, C. J. F. Flipse, R. A. De Groot, and A. Wold, Electronic structure of MoSe₂, MoS₂, and WSe₂. I. Band-structure calculations and photoelectron spectroscopy, *Phys. Rev. B* **35**, 6195 (1987).
- [28] J. J. Yeh and I. Lindau, Atomic subshell photoionization cross sections and asymmetry parameters: 1 ≤ *Z* ≤ 103, *At. Data Nucl. Data Tables* **32**, 1 (1985).
- [29] M. P. Deshpande, G. K. Solanki, and M. K. Agarwal, Optical band gap in tungsten diselenide single crystals intercalated by indium, *Mater. Lett.* **43**, 66 (2000).
- [30] J. A. Wilson and A. D. Yoffe, The transition metal dichalcogenides discussion and interpretation of the observed optical, electrical, and structural properties, *Adv. Phys.* **18**, 193 (1969).
- [31] R. Späh, U. Elrod, M. Lux-Steiner, E. Bucher, and S. Wagner, *pn* junctions in tungsten diselenide, *Appl. Phys. Lett.* **43**, 79 (1983).
- [32] L. C. Upadhyayula, J. J. Loferski, A. Wold, W. Giriat, and R. Kershaw, Semiconducting properties of single crystals of *n*- and *p*-type tungsten diselenide (WSe₂), *J. Appl. Phys.* **39**, 4736 (1968).
- [33] X. Gonze, A brief introduction to the ABINIT software package, *Z. Kristallogr.* **220**, 558 (2005).
- [34] X. Gonze, B. Amadon, P.-M. Anglade, J.-M. Beuken, F. Bottin, P. Boulanger, F. Bruneval *et al.*, ABINIT: First-principles approach to material and nanosystem properties, *Comput. Phys. Commun.* **180**, 2582 (2009).
- [35] G.-B. Liu, W.-Y. Shan, Y. Yao, W. Yao, and D. Xiao, Three-band tight-binding model for monolayers of group-VIB transition metal dichalcogenides, *Phys. Rev. B* **88**, 085433 (2013).
- [36] E. Cappelluti, R. Roldán, J. A. Silva-Guillén, P. Ordejón, and F. Guinea, Tight-binding model and direct-gap/indirect-gap transition in single-layer and multilayer MoS₂, *Phys. Rev. B* **88**, 075409 (2013).

- [37] A. Klein, S. Tiefenbacher, V. Eyert, C. Pettenkofer, and W. Jaegermann, Electronic band structure of single-crystal and single-layer WS₂: Influence of interlayer van der Waals interactions, *Phys. Rev. B* **64**, 205416 (2001).
- [38] Th. Straub, K. Fauth, Th. Finteis, M. Hengsberger, R. Claessen, P. Steiner, S. Hüfner, and P. Blaha, Valence-band maximum in the layered semiconductor WSe₂: Application of constant-energy contour mapping by photoemission, *Phys. Rev. B* **53**, R16152(R) (1996).
- [39] Th. Finteis, M. Hengsberger, Th. Straub, K. Fauth, R. Claessen, P. Auer, P. Steiner *et al.*, Occupied and unoccupied electronic band structure of WSe₂, *Phys. Rev. B* **55**, 10400 (1997).
- [40] Th. Finteis, M. Hengsberger, Th. Straub, K. Fauth, R. Claessen, P. Auer, P. Steiner *et al.*, Erratum: Occupied and unoccupied electronic band structure of WSe₂, *Phys. Rev. B* **55**, 10400(E) (1997); **59**, 2461 (1999).
- [41] M. Traving, M. Boehme, L. Kipp, M. Skibowski, F. Starrost, E. E. Krasovskii, A. Perlov, and W. Schattke, Electronic structure of WSe₂: A combined photoemission and inverse photoemission study, *Phys. Rev. B* **55**, 10392 (1997).
- [42] S.-W. Yu, T. Lischke, R. David, N. Müller, U. Heinzmann, C. Pettenkofer, A. Klein *et al.*, Spin resolved photoemission spectroscopy on WSe₂, *J. Electron Spectrosc. Relat. Phenom.* **101-103**, 449 (1999).
- [43] P. Zhang, P. Richard, T. Qian, Y.-M. Xu, X. Dai, and H. Ding, A precise method for visualizing dispersive features in image plots, *Rev. Sci. Instrum.* **82**, 043712 (2011).
- [44] The estimated error here is a combination of the standard error in parabolic fitting and the standard deviation of the effective mass along different high symmetry directions.
- [45] Based on our DFT-LDA calculation.
- [46] Y. Zhang, T. R. Chang, B. Zhou, Y.-T. Cui, H. Yan, Z. Liu, F. Schmitt *et al.*, Direct observation of the transition from indirect to direct bandgap in atomically thin epitaxial MoSe₂, *Nat. Nanotechnol.* **9**, 111 (2014).
- [47] W. Jin, P.-C. Yeh, N. Zaki, D. Zhang, J. T. Sadowski, A. Al-Mahboob, A. M. van der Zande *et al.*, Direct Measurement of the Thickness-Dependent Electronic Band Structure of MoS₂ Using Angle-Resolved Photoemission Spectroscopy, *Phys. Rev. Lett.* **111**, 106801 (2013).
- [48] K. Kośmider, J. W. González, and J. Fernández-Rossier, Large spin splitting in the conduction band of transition metal dichalcogenide monolayers, *Phys. Rev. B* **88**, 245436 (2013).
- [49] D. Xiao, M.-C. Chang, and Q. Niu, Berry phase effects on electronic properties, *Rev. Mod. Phys.* **82**, 1959 (2010).
- [50] D. Xiao, G. B. Liu, W. Feng, X. Xu, and W. Yao, Coupled Spin and Valley Physics in Monolayers of MoS₂ and Other Group-VI Dichalcogenides, *Phys. Rev. Lett.* **108**, 196802 (2012).
- [51] K. R. Knox, A. Locatelli, M. B. Yilmaz, D. Cvetko, T. O. Menteş, M. Á. Niño, P. Kim, A. Morgante, and R. M. Osgood, Jr., Making angle-resolved photoemission measurements on corrugated monolayer crystals: Suspended exfoliated single-crystal graphene, *Phys. Rev. B* **84**, 115401 (2011).